# JMB

Available online at www.sciencedirect.com

**ScienceDirect**

ELSEVIER

# Steric Zipper of the Amyloid Fibrils Formed by Residues 109–122 of the Syrian Hamster Prion Protein

## Shin-Wen Lee[1], Yun Mou[1], Shu-Yi Lin[1], Fang-Chieh Chou[1], Wei-Hsiang Tseng[1], Chun-hsien Chen[1], Chun-Yi David Lu[1], Steve S.-F. Yu[2] and Jerry C.C. Chan[1]*

[1]*Department of Chemistry, National Taiwan University, No. 1, Section 4, Roosevelt Road, Taipei 106, Taiwan*

[2]*Institute of Chemistry, Academia Sinica, Nankang, Taipei 115, Taiwan*

*Edited by S. Radford*

We report the results of atomic force microscopy, Fourier-transform infrared spectroscopy, solid-state nuclear magnetic resonance, and molecular dynamics (MD) calculations for amyloid fibrils formed by residues 109–122 of the Syrian hamster prion protein (H1). Our data reveal that H1 fibrils contain no more than two β-sheet layers. The peptide strands of H1 fibrils are antiparallel with the A117 residues aligned to form a linear chain in the direction of the fibril axis. The molecular structure of the H1 fibrils, which adopts the motif of steric zipper, is highly uniform in the region of the palindrome sequence AGAAAAGA. The closest distance between the two adjacent β-sheet layers is found to be about 5 Å. The structural features of the molecular model of H1 fibrils obtained by MD simulations are consistent with the experimental results. Overall, our solid-state NMR and MD simulation data indicate that a steric zipper, which was first observed in the crystals of fibril-forming peptides, can be formed in H1 fibrils near the region of the palindrome sequence.

## Introduction

Prions, defined as proteinaceous infectious particles,[1] were first introduced in 1982 to describe a new type of infectious pathogens that propagate through multiple conformers of a normal cellular protein.[2] Prions are composed of a modified isoform of the cellular prion protein (PrP$^C$), which is a constituent of normal mammalian cells. This disease-causing isoform is subsequently known as the scrapie prion protein (PrP$^{Sc}$). There are many fatal

neurodegenerative diseases closely related to prions such as the Creutzfeldt–Jakob disease and bovine spongiform encephalopathy (commonly known as the "mad cow" disease). The molecular structures of PrP$^C$ and some of its variants have been solved by solution-state NMR.[3,4] On the other hand, purified PrP$^{Sc}$ is insoluble and its molecular structure is currently not available. It is nowadays a consensus that the amyloidogenic region from residues 90 to 143 plays a significant role in the conversion from PrP$^C$ to PrP$^{Sc}$.[5] Indeed, it has been shown that the amyloid fibrils formed by the peptide fragments of the mouse PrP$_{89-143}$ can induce prion disease in transgenic mice.[6] Furthermore, secondary-structure analysis indicated that PrP$^C$ contains four α-helices, designated H1–H4.[5,7] Synthetic peptides encompassing the H1 region (109–122) have shown to be highly fibrillogenic and toxic to neurons *in vitro*,[8–11] and they have been used to study prion transmission barrier *in vitro*.[12] Therefore, amyloid fibrils formed by H1 peptides are important biological models for the study of prions. Research studies of amyloid fibrils are being actively pursued because of their occurrence in neurodegenerative diseases.[13] In

*Corresponding author.* E-mail address: chanjcc@ntu.edu.tw.

Abbreviations used: MD, molecular dynamics; PrP$^C$, cellular prion protein; PrP$^{Sc}$, scrapie prion protein; SSNMR, solid-state NMR; FT-IR, Fourier-transform infrared; AFM, atomic force microscopy; CSA, chemical shift anisotropy; MAS, magic-angle spinning; REDOR, rotational-echo double-resonance; fpRFDR-CT, constant time finite-pulse radio frequency-driven recoupling; TFA, trifluoroacetic acid; DI, deionized; TMAFM, tapping mode atomic force microscopy.

particular, solid-state NMR (SSNMR) spectroscopy has been established as a powerful experimental technique for the structural determination of amyloid fibrils.[14–37]

Amyloid fibrils formed by peptides of the H1 region have recently been studied by NMR-detected hydrogen–deuterium exchange measurements and Fourier-transform infrared (FT-IR) spectroscopy,[38–42] which provide valuable structural information concerning the overall organization of the β-sheet structures. However, site-specific structural constraints remain unavailable for this class of amyloid fibrils. In this work, atomic force microscopy (AFM), FT-IR, SSNMR spectroscopy, and molecular dynamics (MD) simulations have been applied to elucidate the structure of the amyloid fibrils formed by residues 109–122 of the Syrian hamster prion protein H1 peptides (Ac-MKHMAGAAAAGAVV-NH$_2$) at site-specific level. The backbone torsion $\psi$ angles and the distances between two stacking β-sheet layers determined by SSNMR are in favorable agreement with those obtained from MD simulations. The results show that the molecular structure of the H1 fibrils adopt the steric-zipper motif recently proposed by Sawaya et al.[43]

## Results

### Fibril morphology

The effect of the imaging forces on the height of topographic features was examined for the fibril samples (Fig. 1). The results suggest that the fibrils are deformed if the tip force is stronger than 10 nN. The heights of the prion fibrils appeared constant when the intermittent vertical force was smaller than 10 nN. Therefore, the working force in this study was carefully maintained under 10 nN. Figure 2a displays a typical AFM image verifying that, after 1-day incubation at 37 °C, the H1 peptides become fibrils with a length of over 400 nm. The fibrils
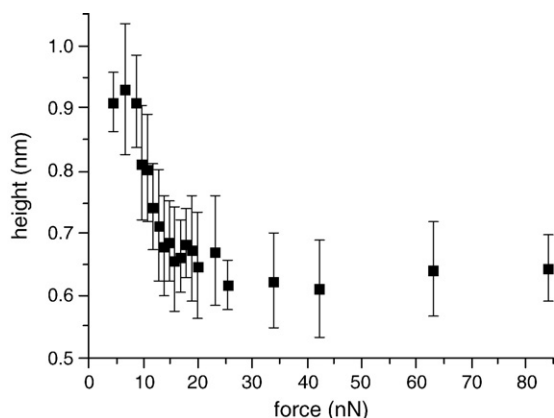
**Fig. 1.** Effect of the intermittent vertical force on the apparent height of the prion fibrils. The standard deviation and average values were measured from five different AFM tips. See Materials and Methods for other details.
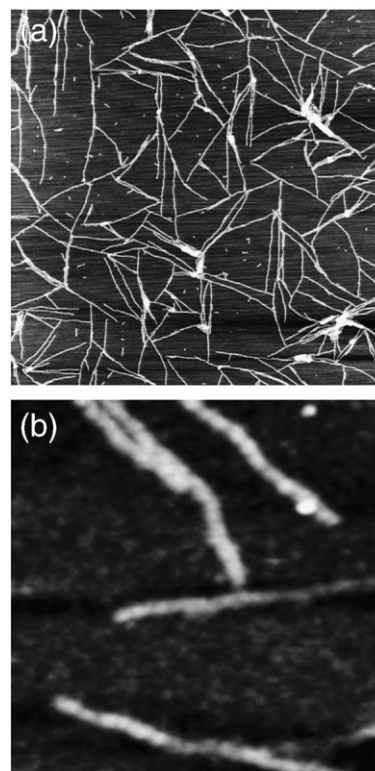
**Fig. 2.** TMAFM images of fibrils on mica in air. Scan size: (a) 2 μm×2 μm, (b) 250 nm×250 nm. The sample was incubated in 37 °C for one day.

exhibit a uniform height of 0.9±0.1 nm, which suggests that the fibril structure does not have more than two β-sheet layers. From the section profiles along the transversal direction of the fibrils, their widths are found to be 11.2±1.3 nm, which, however, are overestimated due to the finite curvature of the AFM tips. To circumvent this problem, the width is obtained from close-packed fibrils, for example, at the upper portion of Fig. 2b. The peak-to-peak distance of the section profile renders a width of ca 9 nm.

### FT-IR measurements

On the basis of IR studies of model peptides, the splitting of the amide I band (consists primarily of CO stretching) into stronger and weaker bands at ca 1630 and 1695 cm$^{-1}$, respectively, has been interpreted as support for antiparallel β-sheet structures.[44] However, such interpretation is not unequivocal for amyloid fibrils.[19,45] On the other hand, it has recently been reported that the amide I band of a singly $^{13}$C-labeled carbonyl site can be used to probe for the β-sheet organization in amyloid fibrils.[39] The isotopic labeling scheme of the samples selected for our FT-IR measurements are summarized in Table 1. Figure 3 shows the transmittance FT-IR spectra measured for six fibril samples in which the carbonyl carbon atoms at A113, G114, A117, G119, A120, and V122 were $^{13}$C labeled. All the $^{13}$C amide I′ bands of our samples occur at about 1612 cm$^{-1}$ except the one of A117,

**Table 1.** Isotopic labeling of H1 fibril samples

| Sample | Labeling scheme | Measurements |
|---|---|---|
| AGV | Uniform $^{15}N$ and $^{13}C$ labeling of A113, G119, V122 | SSNMR |
| GAV | Uniform $^{15}N$ and $^{13}C$ labeling of G114, A117, V121 | SSNMR |
| MA | Uniform $^{15}N$ and $^{13}C$ labeling of M112, A118 | SSNMR |
| KA | Uniform $^{15}N$ and $^{13}C$ labeling of K110, A116 | SSNMR |
| AA | $^{13}C$ labeling of $C^\beta$ at A115 and C′ at A117 | FT-IR/ SSNMR |
| AAA | $^{13}C$ labeling of $C^\alpha$ at A113, $C^\beta$ at A117, and C′ at A120 | FT-IR/ SSNMR |
| GA1 | Equimolar mixture of peptides with $^{13}C$ labeling of C′ at G119 and $^{15}N$ labeling at A120 | FT-IR/ SSNMR |
| GA2 | $^{13}C$ labeling of C′ at G114, $^{15}N$ labeling of N at A120 | FT-IR/ SSNMR |
| AG | $^{13}C$ labeling of C′ at A113, $^{15}N$ labeling of N at G119 | FT-IR/ SSNMR |
| VG | $^{13}C$ labeling of C′ at V122, $^{15}N$ labeling of N at G119 | FT-IR/ SSNMR |

which is at 1604 cm$^{-1}$. Such a red shift, which is due to the coupling of the transition-dipole moments of the amide I modes within the secondary structure,[39] by ca 8 cm$^{-1}$, confirms qualitatively that the hydrophobic core of H1 forms an antiparallel β-sheet conformation, resulting in the alignment of residue A117 in all of the strands.[42] The poor resolution of the spectrum measured for the VG sample is attributed to the structural disorder at the C-terminus, as indicated by the corresponding NMR signal linewidths (vide infra).

## $^{13}C$ chemical shifts and linewidths

NMR chemical shifts and linewidth data obtained from the two-dimensional $^{13}C/^{13}C$ chemical shift correlation spectra are summarized in Table 2. The calculated secondary shifts are shown in Fig. 4. The chemical shift data of the residues from A113 to V121 are consistent with a single β-strand conformation. Furthermore, the full widths at half maximum ($\Delta v_{1/2}$) of the $^{13}C$ signals arising from the residues in the central peptide region are in the range of 1.6–2.8 ppm, which are characteristic of well-structured fibril samples.[19] In comparison, the $\Delta v_{1/2}$ data of the residues K110 and V122 are broader, revealing a considerable structural disorder near the C- and N-termini. It is noteworthy that the residues G114, A116, A117, A118, and G119 have a single sharp peak for each of the carbonyl (C′) and α carbon ($C^\alpha$) signals, whereas the alanine residues (A115–A118) contain two sharp peaks of comparable intensities for the β carbon ($C^\beta$) signal. A typical cross-peak pattern is shown in Fig. 5 for the residue A117. At the first glance, the splitting of the $C^\beta$ signals can be readily attributed to the occurrence of structural polymorphism, which is commonly found in amyloids. According to the SSNMR study of the fibrils formed by the peptide GNNQQNY, the observed polymorphs have distinctive chemical

shifts for all the carbon signals.[37] Therefore, it is not likely that the side chains of the residues GAAAAG of H1 fibrils could adopt two different conformations without affecting the backbone structure. Consequently, our data imply that there are two different quaternary contacts for the methyl groups in GAAAAG.

## Determination of backbone torsion ψ angle

The chemical shift data provide a qualitative identification of the secondary structure of the peptides. To obtain more quantitative structural constraints on the backbone conformation, we have developed an SSNMR pulse sequence to determine the backbone torsion ψ angle of a uniformly labeled residue by correlating the chemical shift anisotropy (CSA) of the C′ and the $^{13}C$–$^1H$ heteronuclear dipole–dipole interaction of the $C^\alpha$.[47] The dihedral angles determined for L-[U-$^{13}C$, $^{15}N$]alanine and *N*-acetyl-DL-[U-$^{13}C$, $^{15}N$]valine under magic-angle spinning (MAS) at 25 kHz are in excellent agreement with the diffraction data.[47–49] For our fibril samples, the C′ CSAs of M112, A113, V121, and V122, which are required for the ψ angle determination, were characterized by the $C^\alpha$-detection method.[50] The principal components of the chemical shift tensors are summarized in Table 3. The C′ CSA determined for A113 is used for the ψ angle analyses of other alanine residues, assuming that the C′ CSAs of all the alanine residues with β-strand conformation are approximately the same. Additional calculations show that the ψ angle analysis is not sensitive to the C′ CSA. Figure 6 shows the total squared deviations between the experimental and simulated data normalized by the mean squared noise ($\chi^2$) as a function of the ψ angle for A117. Reflection symmetries about −60° and 120° are due to the symmetry properties of the C′ CSA and the $C^\alpha$–$H^\alpha$ dipolar interactions.[47,51] Although there are two global minima in the $\chi^2$ plot, the isotropic $^{13}C$ chemical shifts indicate that the ψ angle of A117 is in the β-sheet region (120°–160°), and hence it is estimated to be 156°±3° at the 95.4% confidence level according to the procedure described in the literature.[52] Typical raw data are shown in the Supplementary Data. The ψ angles determined in a similar way for other residues are summarized in Table 4. We find that the ψ angles of the hydrophobic segment are mostly in the region of 150°–160°.

## Organization of the β-sheet structure

In the cross-β structural motif, the registry of the hydrogen bonds between the β strands is determined by a delicate balance of multiple side chain–side chain interactions. Experimentally, the organization of the β-sheet structure can be determined by measuring the distance between two selected residues in adjacent β strands. In this regard, rotational-echo double-resonance (REDOR) is a particularly useful SSNMR technique because REDOR can be used to determine reliably the distance of a $^{13}C$–$^{15}N$
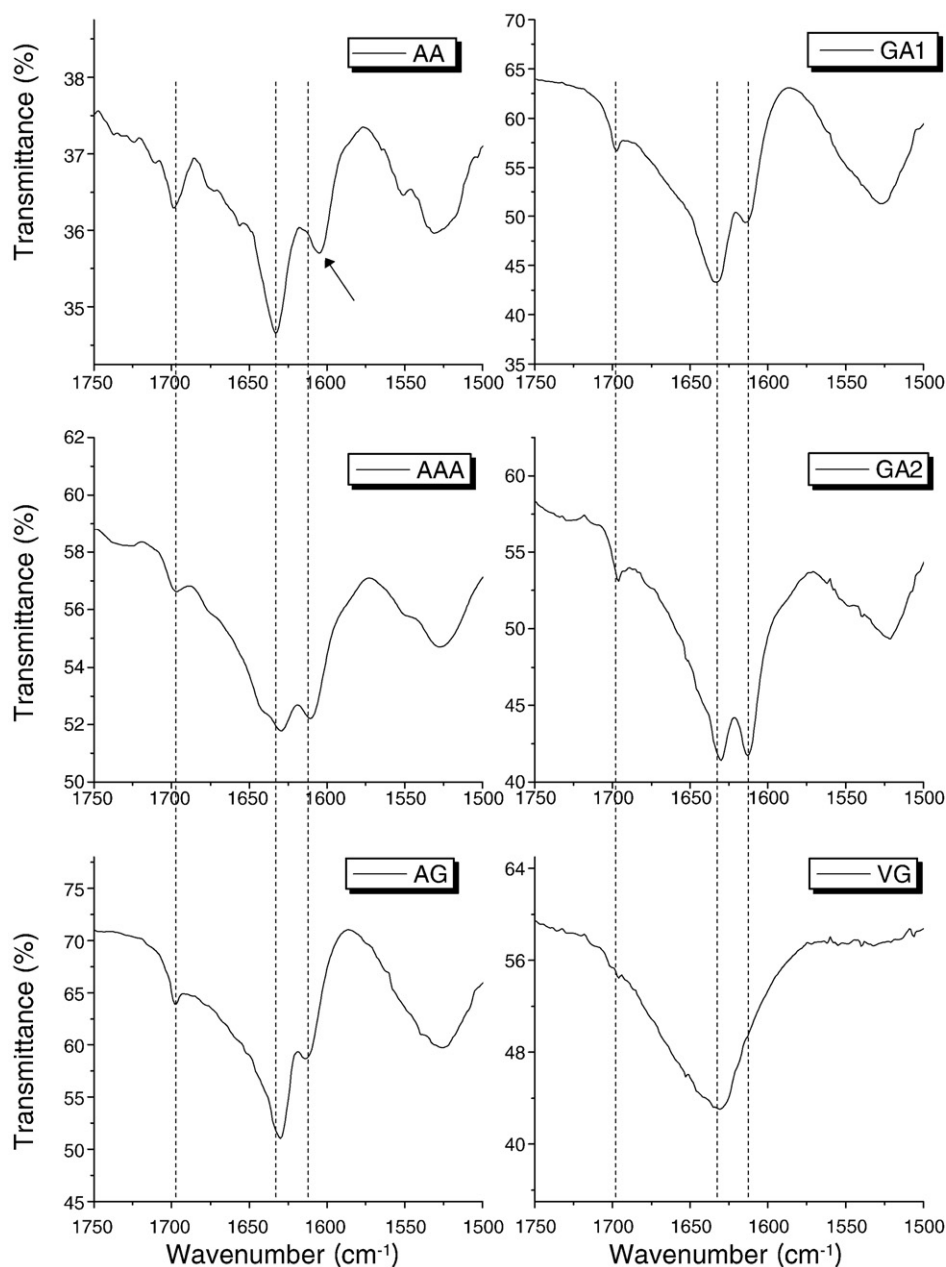
**Fig. 3.** Transmittance FT-IR spectra of $^{13}$C'-labeled fibril samples: AA (A117), AAA (A120), GA1 (G119), GA2 (G114), AG (A113), and VG (V122). The three dashed lines positioned at 1698, 1632, and 1612 cm$^{-1}$ are eye guides. The $^{13}$C amide I' band of A117, highlighted by an arrow, is at 1604 cm$^{-1}$.

spin pair or the geometry of a small spin cluster containing $^{13}$C and $^{15}$N spins.[53] With reference to the FT-IR measurements, the β-sheet structure of our fibril sample is predicted to be antiparallel with the A117 residues aligned to form a linear chain in the direction of the fibril axis. To verify this antiparallel model, we measured the $^{13}$C{$^{15}$N} REDOR data of the GA2 sample ($^{15}$N-A120/$^{13}$C'-G114). We carried out a series of numerical simulations on a $^{15}$N–$^{13}$C–$^{15}$N system, in which the two $^{15}$N–$^{13}$C distances ($r_1 \leq r_2$) and the NCN angle (θ) were taken as three independent variables. Figure 7 shows some of the simulation results and the experimental REDOR data corrected for the contribution due to natural

abundance signals.[54] From the three-dimensional $\chi^2$ plot (not shown), $r_1$, $r_2$, and θ are determined to be 4.2–4.7°, 4.7–6.0°, and 150–170°, respectively, at the 68.3% confidence level. The REDOR data are consistent with the antiparallel model.

To probe for the internuclear distance between the $^{13}$C nuclei in close proximity, we employed the $^{13}$C constant-time finite-pulse radio frequency-driven recoupling (fpRFDR-CT) technique,[55] which has been successfully applied to the studies of amyloid fibrils.[17] The experimental data measured for 1-$^{13}$C-L-alanine were used to validate the implementation of the fpRFDR-CT technique in our spectrometer (Supplementary Data). For the study of H1 fibrils,

**Table 2.** $^{13}C$ NMR chemical shift and linewidth data (ppm) for $^{13}C$- and $^{15}N$-labeled sites in H1 fibrils

| Residue | C′ δ, $\Delta v_{1/2}$ | C$^\alpha$ δ, $\Delta v_{1/2}$ | C$^\beta$ δ, $\Delta v_{1/2}$ | C$^\gamma$ δ, $\Delta v_{1/2}$ | C$^\delta$ δ, $\Delta v_{1/2}$ | C$^\kappa$ δ, $\Delta v_{1/2}$ | Sample |
|---|---|---|---|---|---|---|---|
| K110 | 174.2, 3.4 | 57.0, 3.8, 42% <br> 54.1, 3.6, 58% | 32.3, 3.8 | 24.7, 1.7 | 28.5, 3.4 | 41.3, 2.5 | KA |
| M112 | 173.0, 2.9 | 56.0, 2.9, 40% <br> 53.7, 2.2, 60% | 32.0, 5.1, 56% <br> 36.0, 4.2, 44% | —, — | 16.7, 2.0 | —, — | MA |
| A113 | 173.3, 2.0 | 49.4, 2.2 | 20.5, 3.0 | | | | AGV |
| G114 | 168.4, 1.9 | 43.5, 2.2 | | | | | GAV |
| A115 | | | 20.9, 2.7, 68% <br> 23.4, 2.1, 32% | | | | AA |
| A116 | 173.5, 1.8 | 50.3, 1.9 | 23.3, 1.9, 50% <br> 21.8, 1.6, 50% | | | | KA |
| A117 | 172.6, 2.0 | 49.4, 1.7 | 23.3, 2.0, 44% <br> 21.0, 1.6, 56% | | | | GAV |
| A118 | 174.3, 1.9 | 50.5, 1.9 | 24.9, 1.7, 35% <br> 22.5, 2.0, 65% | | | | MA |
| G119 | 168.4, 1.8 | 43.3, 2.1 | | | | | AGV |
| V121 | 171.8, 2.9, 57% <br> 170.0, 3.1, 43% | 59.0, 2.4, 39% <br> 57.5, 2.0, 61% | 34.8, 1.8, 31% <br> 33.5, 2.2, 69% | 19.8, 2.0, 67% <br> 17.6, 3.2, 32% | | | GAV |
| V122 | 175.2, 3.0 | 58.8, 2.6, 28% <br> 57.1, 3.7, 72% | 32.7, 2.8, 58% <br> 34.1, 2.3, 42% | 19.6, 2.9 | | | AGV |

The chemical shift data uncertainty is typically 0.3 ppm for $\Delta v_{1/2} \leq 3$ ppm. In the presence of multiple peaks, their relative signal integrals are given in percentage.

we prepared the fibril sample AAA with $^{13}C^\beta$ label at A117, $^{13}C'$ labeling at A120, and $^{13}C^\alpha$ labeling at A113. Experimentally, we indeed observed a significant attenuation of the $^{13}C^\beta$ signal as a function of the dephasing time. For a single β-sheet layer,
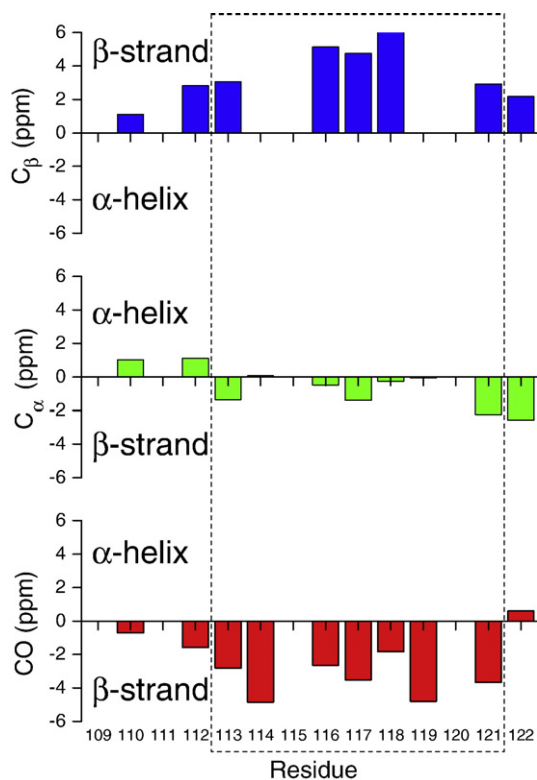


**Fig. 4.** Secondary chemical shifts calculated for selected residues of the fibril samples. The rectangular dashed line highlights the region of which the shifts are consistent with the β-sheet conformation. The random-coiled values were obtained from Ref. 46.

such significant signal attenuation is possible only if the methyl groups of neighboring A117 residues are pointing in the same direction, forming a linear chain along the fibril axis. To quantify the spacing between the β-strands, the $^{13}C^\beta$ fpRFDR-CT data of A117 are compared with simulations on a linear chain of six spins with $d$ varied from 4.7 to 6.7 Å. The contribution from the natural abundance signals were corrected for using the procedure described in the literature.[17] From the corresponding $\chi^2$ plot, $d$ is determined to be $5.3 \pm 0.2$ Å at 90% confidence level. Again, this result is consistent with the antiparallel model. For comparison, we also analyzed the data by a two-spin model, in which $d$ is determined to be $4.8 \pm 0.5$ Å at 90% confidence level. This result indicates that the signal dephasing in the $^{13}C$ fpRFDR-CT experiment is dominated by two neighboring spins for a linear chain of spin species.

**Distance between pairs of β-sheets**

For the AAA sample, we also measured the fpRFDR-CT data of the C$^\alpha$ and C′ signals. The intensity of the C$^\alpha$ signal is very weak, presumably due to insufficient proton decoupling. With reference to the antiparallel model, the C′ signal should have no signal attenuation because the distance between the C′ nuclei of two nearest A120 residues is larger than 20 Å. The same is also expected for the C′ signal of the GA2, AG, and VG samples. To our surprise, the converse was observed experimentally. Because the fibril sample has a uniform height of $0.9 \pm 0.1$ nm, we hypothesize that the protofilament of our fibril sample contains two β-sheet layers in close proximity. That is, the protofilament contains a hydrophobic core formed by two β-sheet layers mated tightly together. Thus, the observed signal attenuation of the C′ is due to the labeled residues in adjacent β-sheet layers. This hypothesis is not unreasonable
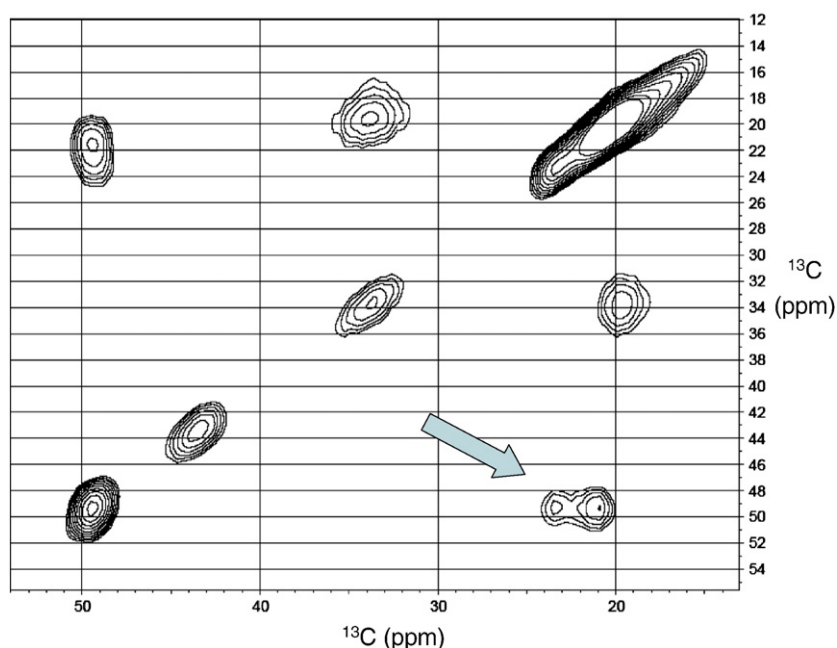
**Fig. 5.** $^{13}C–^{13}C$ correlation spectrum obtained for the GAV sample. The arrow indicates the $C^\alpha \rightarrow C^\beta$ cross-peaks for the A117 residue, from which we conclude that there are two different $C^\beta$ peaks but one $C^\alpha$ peak for the A117 residue. Spectral deconvolution shows that the volume ratio of the two peaks is 44:56.

because the residues from 113 to 120 comprise Gly and Ala only, which allows a close contact between two β-sheet layers. This so-called "pair-of-sheets" motif has been suggested as the fundamental unit of amyloid-like fibrils.[43,56] The observation of two $C^\beta$ signals in the GAAAAG region, as discussed in the foregoing section, could thus be attributed to the Ala residues whose side chains are located in and outside the hydrophobic core.

On the basis of our structural hypothesis, we analyze the $^{13}C^\beta$ fpRFDR-CT data of AA, and the $^{13}C'$ fpRFDR-CT data of the AAA, GA2, AG, and VG samples, by a two-spin system (Fig. 8). From the corresponding $\chi^2$ plots, the distances between the two β-sheet layers were determined and are summarized in Table 5. The closest distance between the two adjacent β-sheet layers is found to be ca 5 Å. In principle, one may measure the REDOR data of the GA1 sample to probe for the layer distance. However, preliminary data show that there are considerable dynamics between the two layers in the NMR time scale, rendering the quantitative analysis of the REDOR data very difficult. On the other hand, Balbach *et al.* have demonstrated by

simulations that fpRFDR-CT is applicable to the case where the spin–spin relaxation time is larger than or equal to 30 ms.[17]

## MD simulations

The AFM and NMR data imply that the structure of H1 fibrils is composed of two β-sheet layers. Very recently, Sawaya *et al.*[43] and Nelson *et al.*[56] have reported the atomic-level structures for 13 short peptide segments (four to seven residues) of fibril-forming proteins, from which the term "steric zipper" is coined to describe the dry surface between two tightly interdigitated β-sheets. To

**Table 3.** Principal components of selected C′ chemical shift tensors of H1 fibril samples

| Residue | $\delta_{11}$ (ppm) | $\delta_{22}$ (ppm) | $\delta_{33}$ (ppm) |
|---------|-----|-----|-----|
| M112 | 239 | 181 | 98 |
| A113 | 243 | 180 | 97 |
| V121 | 241 | 178 | 93 |
| V122 | 244 | 186 | 95 |

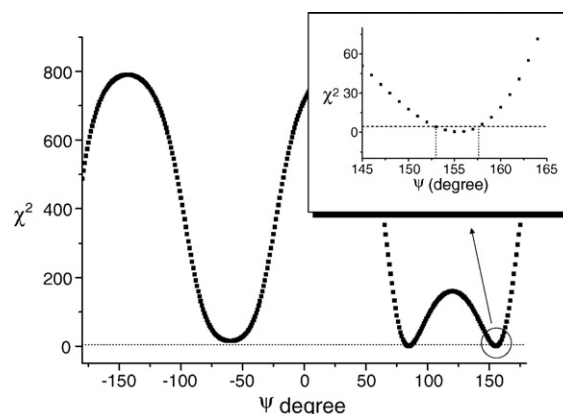The corresponding data reported in Ref. 50 are mislabeled.



**Fig. 6.** Total squared deviations ($\chi^2$) between experimental and simulated data normalized by mean squared noise as a function of the backbone ψ angle. The horizontal dashed line indicates the 95.4% confidence limits. The inset highlights the data near the β-sheet region.

**Table 4.** Summary of the experimental and simulated backbone torsion angle $\psi$ of selected residues in H1 fibrils

| Residue | NMR experiments[a] | MD simulations[b] |
|---|---|---|
| M109 | — | 45±46 |
| K110 | — | 55±29 |
| H111 | — | 94±68 |
| M112 | 157±10 | 140±12 |
| | 171±9 | |
| A113 | 158±3 | 161±5 |
| G114 | — | 161±9 |
| A115 | — | 157±4 |
| A116 | 155±5 | 153±3 |
| A117 | 156±3 | 153±3 |
| A118 | 157±5 | 158±3 |
| G119 | — | 161±9 |
| A120 | — | 155±3 |
| V121[c] | 151±5 | 131±13 |
| V122[c] | 150±5 | 57±50 |

[a] The error bars reflect the boundaries at the 95.4% confidence level.
[b] The error bars correspond to the standard deviations of the average $\psi$ values of the eight residues over the last 2/3 of the NVT simulation time course.
[c] Averaged values determined for multiple conformations.

investigate the likelihood of finding a steric zipper in H1 fibrils, we have carried out MD simulations on an octamer of the H1 peptide. The initial configuration of the octamer was prepared as described in Materials and Methods. Energy minimization was done to relax local strains. The octamer was then placed in a rectangular box under periodic boundary condition and MD simulations were conducted in the NPT ensemble (constant number of particles, 1 atm, 300 K) for 190 ps. The equilibrium value of the box dimension along the fibril long axis was found to be 18.3 Å. To simulate an isolated and infinitely long fibril, the subsequent simulation in the NVT ensemble (constant number of particles, 150 × 150 × 18.3 Å, 300 K) was performed for 2 ns, in which the fibril long axis was parallel to the z-axis. The overall fibril structure is stable in the course of the NVT
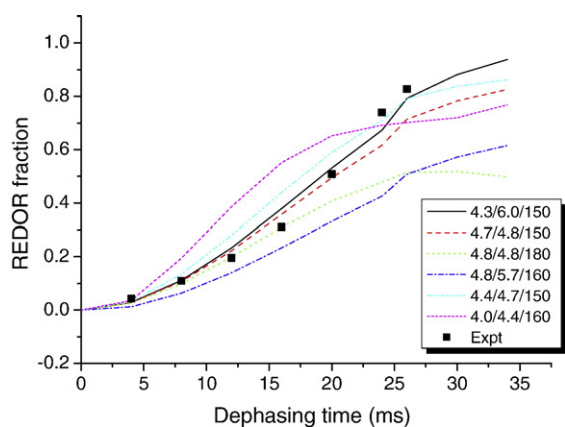


**Fig. 7.** Experimental $^{13}C\{^{15}N\}$ REDOR data of the GA2 sample. The lines are simulations based on selected structural parameters $r_1/r_2/\theta$ of an $^{15}N–^{13}C–^{15}N$ system, in which the two $^{15}N–^{13}C$ distances ($r_1 \leq r_2$) and the NCN angle ($\theta$) were taken as three independent variables.
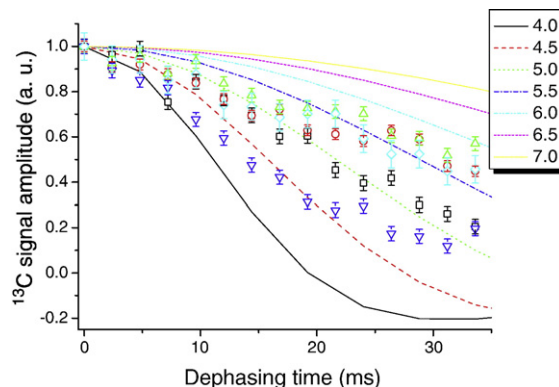


**Fig. 8.** $^{13}C$ fpRFDR-CT data of the AA ($C^\beta$, ▽), AAA ($C'$, □), GA2 ($C'$, ○), AG ($C'$, △), and VG ($C'$, ◊) samples. The lines are simulations on a two-spin system at different distances in angstroms.

simulation. The two antiparallel β-sheets form a stable layer structure with a layer–layer distance of ca 5 Å. The average backbone torsion $\psi$ angles and the layer distances are summarized and compared with the NMR data in Tables 4 and 5, where a good agreement is obtained in the central region of the fibril. It is noteworthy that no NMR constraints were added in the whole course of MD simulations. The time evolution of the energy of the fibril structure is shown in the Supplementary Data.

## Discussion

### Backbone torsion ψ angle determination

Backbone torsion angles can be accurately estimated by measuring the $^{13}C$ and $^{15}N$ secondary chemical shifts on the basis of the TALOS approach.[57] However, this empirical approach is not very useful for the characterization of secondary structures such as a bend or turn, which has been shown to be an important motif in amyloid fibrils.[19,32] There are many different SSNMR techniques suggested for the direct determination of peptide backbone torsion angles $\phi$ and $\psi$ under MAS.[58–62] Most of the techniques, however, require isotopic labeling of two consecutive residues for the determination of a single pair of backbone torsion angles.[63–70] Very recently, we have developed a SSNMR technique to

**Table 5.** Summary of the experimental and simulated distances of selected spin pairs in H1 fibrils

| Spin pairs | NMR experiments[a] | MD simulations |
|---|---|---|
| C′(A113)–C′(A113) | 6.0±0.6 | 6.02±0.57 |
| C′(G114)–C′(G114) | 5.9±0.6 | 5.17±0.43 |
| C$^\beta$(A115)–C$^\beta$(A115) | 4.9±0. 5 | 5.42±0.26 |
| C′(A120)–C′(A120) | 5.3±0.6 | 6.19±0.54 |
| C′(V122)–C′(V122) | 5.8±0.5 | 10±1 |

[a] The error bars reflect the boundaries at the 90% confidence level.

quantify the backbone torsion $\psi$ angle of a singly uniformly labeled residue in polypeptides.[47,71] This technique has been successfully applied to the study of our target prion fibrils, from which we obtain site-specific structural constraints in the hydrophobic segment. Although the data measured for our fibril samples all fall in the region of β-sheet conformation, our technique is readily applied to the study of other secondary structures. Overall, our results are consistent with the earlier SSNMR data measured for the fibrils formed by the P101L mutant sequence of PrP$_{89-143}$, which reveal that the 112–124 segment adopts an extended β-sheet conformation.[16,33]

## Structural model for H1 fibrils

The steric-zipper motif was deduced from the X-ray crystallographic studies of microcrystals formed by fibril-forming peptides.[43,56] It remains to be resolved how close the structure of the microcrystals is to that of the corresponding fibrils. Nevertheless, our AFM and SSNMR data lend a strong support to the formation of steric zipper for the H1 fibrils. According to the classification scheme of Sawaya *et al.*, there are eight possible classes of steric zipper.[43] The FT-IR data provide a very strong constraint that the individual β-sheet layer of H1 fibrils is antiparallel. Without the FT-IR data, it is not easy to distinguish whether the fpRFDR-CT and REDOR data reveal the layer–layer distance or the interstrand distance within an individual β-sheet. Together with the fact that there are two different quaternary contacts for the methyl groups in the region GAAAAG, our data are consistent with the so-called class 6, 7, and 8 steric zippers.[43] As an illustration of the steric zipper formed by H1 fibrils, we subjectively chose to carry out MD simulations on the H1 fibril based on the class 6 steric zipper. At the current stage, our experimental data cannot rule out the possibility that all the three classes of steric zipper are present in H1 fibrils. A snapshot of the equilibrium fibril structure taken from the NVT simulations is shown in Fig. 9. Accordingly, a steric zipper is formed in the β-sheet region of the four consecutive alanine residues (A115–A118), where the side chains of the alanine residues are tightly interdigitated. Our MD simulations are partially validated by the favorable agreement of the calculated structural parameters and the NMR data in the region of the steric zipper.

## Comparison with MoPrP106–126 fibrils

Recently, MD simulations have been used to model the MoPrP106–126 fibrils.[38] The peptide sequence of MoPrP106–126 (TNVKHVAGAAAA-GAVVGGLGG) is quite similar to our H1 sequence, in the sense that the sequence contains two positively charged residues (K109 and H110) near the N-terminus and an uninterrupted hydrophobic region stretching to the amidated C-terminus. Interestingly, the authors found that the octamer formed by two layers of antiparallel β-sheet are unstable and would collapse quickly into irregular globular structures in the course of the MD simulation. Their simulations predict a parallel arrangement within each β-sheet and between the two layers.[38] On the contrary, our MD simulations indicate that two antiparallel β-sheets can form stable layer structure and a similar conclusion is also reported in the study of alanine-rich peptides.[72] Additional simulations are required to clarify whether the apparent discrepancy is due to the difference in the calculation methods or it actually reveals the subtle but dramatic effect of the peptide sequence to fibrillogenesis. In any case, both studies demonstrate that the amyloid fibrils formed by peptides containing the palindrome sequence AGAAAAGA have a strong propensity to adopt the motif of steric zipper.

## Conclusion

Structural determination of steric zipper by SSNMR method is not straightforward, particularly
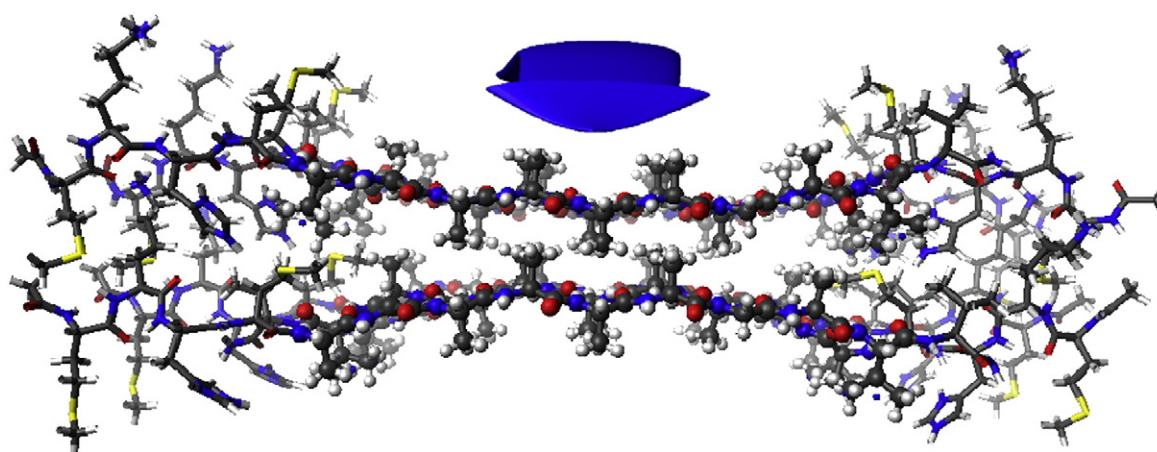


**Fig. 9.** Structural model of the H1 fibrils. The atoms of the residues in the β-sheet region are represented by balls and sticks. The arrow indicates the direction of the fibril axis.

when the distance between two β-sheet layers is comparable to the interstrand distance within the individual β-sheet layer. We show that isotope-edited FT-IR measurements can be carried out for solid fibril samples and provide a very useful structural constraint on which the SSNMR data can be unequivocally analyzed. Our experimental and MD simulation data indicate that a steric zipper, which was first observed in the crystals of fibril-forming peptides, can be formed in H1 fibrils near the region of the palindrome sequence. The two antiparallel β-sheets form a stable layer structure with a layer–layer distance of ca 5 Å in the steric zipper, where the structural order is significantly higher than those near the C- and N-termini.

# Materials and Methods

## Sample preparation and characterization

All the chemicals were obtained from NovaBiochem unless stated otherwise. H1 peptides, with the sequence Ac-MKHMAGAAAAGAVV-NH$_2$, were synthesized on a PS3 (Rainin) peptide synthesizer, using a Rink amide resin (0.6 meq/g substitution level; Novabiochem), and 9-fluorenylmethoxycarbonyl chemistry with 2-(1*H*-benzotriazole-1-yl)-1,1,3,3-tetramethyluronium hexafluorophosphate activation. The synthesis scale was 0.1 mmol, with a fivefold excess and a 2-h coupling time for each unlabeled amino acid, and a twofold excess and a 4-h coupling time for each labeled amino acid. Crude peptides were cleaved from the synthesis resin using standard protocols [reaction for 120 min in 94% trifluoroacetic acid (TFA) with 2.5% ethanedithiol, 2.5% deionized (DI) water and 1% thioanisole scavengers], which were then precipitated in cold *tert*-butyl methyl ether. Precipitated peptides were washed three times with cold *tert*-butyl methyl ether and then lyophilized. The crude material was purified by high-performance liquid chromatography at 50 °C, using a water/acetonitrile gradient with 0.1% TFA and a preparative-scale Vydac C18 reverse-phase column. Samples of 6 mg per injection were dissolved in 100 μL TFA and then diluted to 5 mL with 10% acetonitrile in DI water before being injected into the column. Fractions containing H1 were collected at the concentration of 23% acetonitrile and were frozen in liquid nitrogen immediately after being collected. Peptide purity was at least 90% as determined by matrix-assisted laser desorption/ionization time-of-flight mass spectrometry. The yield of purified peptide, relative to the 0.1 mmol synthesis scale, was approximately 25%. Samples for SSNMR measurements were isotopically labeled at selected positions as summarized in Table 1. $^{13}$C- and $^{15}$N-labeled amino acids with 9-fluorenyl-methoxycarbonyl protection were obtained from Cambridge Isotope Laboratories, CortecNet, and Isotec. Fibril samples were formed by dissolution of purified H1 at a peptide concentration of 754 μM in 100 mM NaCl and 20 mM Hepes buffer (pH 7.4), with addition of 0.01% NaN$_3$. Dissolution was assisted by sonication. Fibrils formed after incubation at 37 °C for 1 day, appearing as a visible precipitate. For SSNMR measurements, the salts were subsequently removed by repeated dissolution in DI water, centrifuged three times, and then lyophilized.

## Tapping mode atomic force microscopy

Tapping mode atomic force microscopy (TMAFM) measurements were carried out with a NanoScope IIIa controller equipped with a Quadrex Electronics extender module (Veeco Metrology Group/Digital Instruments, Santa Barbara, CA). The images were acquired in ambient conditions and with commercially available non-contact silicon cantilevers whose force constant, resonance frequency, and curvature of the tip radius were nominally 42 N/m, 320 kHz, and ≤10 nm, respectively (NCHR, NanoWorld, Switzerland). The scan rates were slower than 4 Hz per imaging line (ca >2 min per frame). The microscope was housed in a homemade vibration–isolation stage. The samples for TMAFM measurements were prepared by 10-fold dilution of the incubated prion (0.75 mM) with 200 μL acetic acid (w/w 1%). Approximately 10 μL of the prion sample was drop-cast onto freshly cleaved mica for 1 min. The solution was then removed and the mica was dried gently with a stream of N$_2$ gas. The sample was subjected to vacuum drying (∼1 h, <120 mTorr) prior to imaging.

## FT-IR measurements

Transmittance FT-IR spectra were collected using a Perkin Elmer (Spectrum 100) spectrometer (series II) in the range of 1000–4000 cm$^{-1}$. The samples were recorded in KBr pellets at room temperature. The frequency scale was calibrated with the measurement of succinic acid.

## Solid-state NMR measurements

All NMR experiments were carried out at $^{13}$C and $^1$H frequencies of 75.5 and 300.1 MHz, respectively, on a Bruker DSX300 NMR spectrometer equipped with a commercial 2.5-mm triple-resonance probe. The MAS frequency variation was limited to ±2 Hz using a commercial pneumatic control unit (Bruker, MAS II). Each fibrillized sample of approximately 6 mg was confined in the middle one-half of the rotor volume with Teflon spacers. Typically, during the cross-polarization contact time (1.5 ms), the $^1$H nutation frequency was set to 50 kHz and that of $^{13}$C was ramped through the Hartmann–Hahn matching condition.[73,74] Unless stated otherwise, continuous-wave and XiX[75] proton decouplings of 100 kHz were applied during recoupling periods and the $t_2$ acquisition, respectively. To reduce the sample heating due to fast MAS, a stream of dry cooling air at −11 °C (800 L/h) was used to keep the sample temperature at around 30 °C, calibrated by measurements on lead (II) nitrate. $^{13}$C NMR chemical shifts were referenced to tetramethylsilane, using adamantane as the secondary reference standard.

$^{13}$C/$^{13}$C chemical shift correlation spectra were measured at a MAS frequency of 25.0 kHz based on the finite-pulse radio frequency-driven recoupling (fpRFDR) technique.[76] During the fpRFDR recoupling periods, the $^{13}$C π pulses were 12 μs ($\tau_p/\tau_r = 0.3$). Chemical shift and linewidth data were obtained by fitting each cross-peak to a Gaussian using the package NMRPipe.[77] Experiments for ψ angle determination were carried out at a MAS frequency of 25 kHz. The π/2 Gaussian selective pulse was set to 200 μs and positioned at the aliphatic region. The $^{13}$C nutation frequencies were set to 60 and 125 kHz for $R12_5^4$ and for the R-TOBSY pulse block, respectively, as required by the pulse symmetries.[78,79] The R-TOBSY

mixing time was set to 7.68 ms, during which no proton decoupling was applied.[80] The Lee–Goldburg irradiation was achieved by setting the $^1$H decoupling field and the resonance offset at 81.6 and 57.8 kHz, respectively, so that the effective nutation frequency was equal to 100 kHz.[81] The duration of the Lee–Goldburg irradiation was fixed to three rotor periods. A more detailed description of the method was given elsewhere.[47] Typically, the total acquisition time for each sample was 96 h, using a 3-s recycle delay.

$^{13}$C{$^{15}$N} REDOR measurements were carried out with active rotor synchronization of π pulses on the $^{15}$N and $^{13}$C channels. The $^{13}$C and $^{15}$N π pulse lengths were set to 6.8 and 18 μs, respectively. The pulse sequence developed by Anderson *et al.* was employed at a MAS frequency of 8.00 kHz.[53,82] The power level of the $^{15}$N π pulses was optimized by maximizing the REDOR dephasing effect. $^1$H TPPM decoupling[83] at 120 and 100 kHz was applied during the recoupling period and the acquisition period, respectively. To enhance data reproducibility, the memory buffer for acquisition was manipulated in such a way that the odd- and even-numbered scans were accumulated separately for the REDOR (S) and spin–echo ($S_0$) signals, respectively. The number of transients accumulated for each fid was 512. Total acquisition time for each of the REDOR data set was ca 5 h, using a 2-s recycle delay.

$^{13}$C–$^{13}$C dipolar recoupling measurements were carried out with the fpRFDR-CT technique[55,76] at a MAS frequency of 20.0 kHz. During the fpRFDR recoupling periods, the $^{13}$C π pulses were set to 15 μs. The $^{13}$C π/2 pulses flanking the fpRFDR pulse blocks were set to 4 μs.[55] The effective dipolar dephasing period was from 0 to 33.6 ms in steps of 2.4 ms. Continuous-wave proton decoupling was 130 kHz during the recoupling period. The C′ and C$^β$ fpRFDR-CT data were obtained separately by placing the rf transmitter frequency near the C′ and C$^β$ signal, respectively. The number of transients accumulated for each fid was 256. Total acquisition time for each of the fpRFDR-CT data sets was ca 4 h, using a 3-s recycle delay.

### Numerical analysis of NMR data

Numerical simulations were carried out using the package SIMPSON (version 1.1.0)[84] and SPINEVOLUTION (version 3.0).[85] The maximum time step over which the Hamiltonian is approximated to be time-independent was set to 1.0 or 2.0 μs. Typically, a powder averaging scheme containing 100 REPULSION angles (α and β)[86] and 18 γ angles was chosen. Relaxation effects were ignored. The simulations for the backbone torsion angle determination were done on a three-spin (C′, C$^α$, H$^α$) system as described earlier.[47] The REDOR data of the GA2 sample were simulated on a three-spin (N, C′, N) system, whereas the $^{13}$C′ fpRFDR-CT data of the AAA, AA, GA2, AG, and VG samples were simulated on a two-spin system. For the analysis of the $^{13}$C$^β$ fpRFDR-CT data of A117, the SPINEVOLUTION simulations were done on a linear chain of six $^{13}$C nuclei, with initial $^{13}$C spin polarization on the central two spins.[25]

### MD simulations

MD simulations were carried out using the program TINKER (version 4.2).[87] All atoms of the systems were considered explicitly, and their interactions were calculated by using the Amber99 force field.[88] The solvent-accessible surface area approach was chosen as our solvent model.[89] A distance cutoff of 9 Å was set for all non-bonded interactions. Long-range electrostatic interactions were evaluated by the smooth particle-mesh Ewald method.[90] The RATTLE algorithm was used to constrain all chemical bonds containing H atoms to their ideal bond lengths.[91] The time step in the MD simulations was set to 2 fs. The fibril model was constructed as follows. An antiparallel β-sheet was formed by four H1 peptides with A117 in register, where the residues K110 were protonated; Cl$^-$ ions were added to maintain charge neutrality; the interstrand distance was set to 4.8 Å; and the backbone torsion angles of all the residues were restrained to ϕ and ψ values of −140° and 140°, respectively. Another similarly prepared β-sheet was then stacked in a parallel fashion, resulting in a layer distance of 7 Å (Supplementary Data). The overall structural configuration conforms to the "class 6" of steric zipper.[43] After energy minimization, MD simulations under periodic boundary condition were performed in the NPT ensemble for 190 ps, followed by simulations in the NVT ensemble for 2 ns. The average backbone torsion ψ angle of each residue was obtained by analyzing the trajectories of all the monomers of the NVT simulation at equilibrium states.

## Supplementary Data

Supplementary data associated with this article can be found, in the online version, at doi:10.1016/j.jmb.2008.03.035

## References

1. Prusiner, S. B. (1998). Prions. *Proc. Natl. Acad. Sci. USA*, **95**, 13363–13383.
2. Prusiner, S. B. (1982). Novel proteinaceous infectious particles cause scrapie. *Science (Washington, D. C.)*, **216**, 136–144.
3. Donne, D. G., Viles, J. H., Groth, D., Mehlhorn, I., James, T. L., Cohen, F. E. *et al.* (1997). Structure of the recombinant full-length hamster prion protein PrP (29–231): the N terminus is highly flexible. *Proc. Natl. Acad. Sci. USA*, **94**, 13452–13457.
4. Riek, R., Hornemann, S., Wider, G., Glockshuber, R. & Wuthrich, K. (1997). NMR characterization of the full-length recombinant murine prion protein, mPrP (23–231). *FEBS Lett.* **413**, 282–288.
5. Huang, Z. W., Prusiner, S. B. & Cohen, F. E. (1996). Scrapie prions: a three-dimensional model of an infectious fragment. *Folding Des.* **1**, 13–19.
6. Kaneko, K., Ball, H. L., Wille, H., Zhang, H., Groth, D., Torchia, M. *et al.* (2000). A synthetic peptide initiates Gerstmann–Straussler–Scheinker (GSS) disease in transgenic mice. *J. Mol. Biol.* **295**, 997–1007.
7. Huang, Z. W., Gabriel, J. M., Baldwin, M. A., Fletterick, R. J., Prusiner, S. B. & Cohen, F. E. (1994).

Proposed 3-dimensional structure for the cellular prion protein. *Proc. Natl. Acad. Sci. USA*, **91**, 7139–7143.

8.  Brown, D. R., Schmidt, B. & Kretzschmar, H. A. (1996). Role of microglia and host prion protein in neurotoxicity of a prion protein fragment. *Nature*, **380**, 345–347.

9.  Forloni, G., Angeretti, N., Chiesa, R., Monzani, E., Salmona, M., Bugiani, O. & Tagliavini, F. (1993). Neurotoxicity of a prion protein-fragment. *Nature*, **362**, 543–546.

10. Jobling, M. F., Stewart, L. R., White, A. R., McLean, C., Friedhuber, A., Maher, F. *et al.* (1999). The hydrophobic core sequence modulates the neurotoxic and secondary structure properties of the prion peptide 106–126. *J. Neurochem.* **73**, 1557–1565.

11. Tagliavini, F., Prelli, F., Verga, L., Giaccone, G., Sarma, R., Gorevic, P. *et al.* (1993). Synthetic peptides homologous to prion protein residues 106–147 form amyloid-like fibrils in-vitro. *Proc. Natl. Acad. Sci. USA*, **90**, 9678–9682.

12. Lee, L. Y.-L. & Chen, R. P.-Y. (2007). Quantifying the sequence-dependent species barrier between hamster and mouse prions. *J. Am. Chem. Soc.* **129**, 1644–1652.

13. Dobson, C. M. (2003). Protein folding and misfolding. *Nature*, **426**, 884–890.

14. Antzutkin, O. N., Balbach, J. J., Leapman, R. D., Rizzo, N. W., Reed, J. & Tycko, R. (2000). Multiple quantum solid-state NMR indicates a parallel, not antiparallel, organization of beta-sheets in Alzheimer's beta-amyloid fibrils. *Proc. Natl. Acad. Sci. USA*, **97**, 13045–13050.

15. Kamihira, M., Naito, A., Tuzi, S., Nosaka, A. Y. & Saito, H. (2000). Conformational transitions and fibrillation mechanism of human calcitonin as studied by high-resolution solid-state C-13 NMR. *Protein Sci.* **9**, 867–877.

16. Laws, D. D., Bitter, H. M. L., Liu, K., Ball, H. L., Kaneko, K., Wille, H. *et al.* (2001). Solid-state NMR studies of the secondary structure of a mutant prion protein fragment of 55 residues that induces neurodegeneration. *Proc. Natl. Acad. Sci. USA*, **98**, 11686–11690.

17. Balbach, J. J., Petkova, A. T., Oyler, N. A., Antzutkin, O. N., Gordon, D. J., Meredith, S. C. & Tycko, R. (2002). Supramolecular structure in full-length Alzheimer's beta-amyloid fibrils: evidence for a parallel beta-sheet organization from solid-state nuclear magnetic resonance. *Biophys. J.* **83**, 1205–1216.

18. Jaroniec, C. P., MacPhee, C. E., Astrof, N. S., Dobson, C. M. & Griffin, R. G. (2002). Molecular conformation of a peptide fragment of transthyretin in an amyloid fibril. *Proc. Natl. Acad. Sci. USA*, **99**, 16748–16753.

19. Petkova, A. T., Ishii, Y., Balbach, J. J., Antzutkin, O. N., Leapman, R. D., Delaglio, F. & Tycko, R. (2002). A structural model for Alzheimer's beta-amyloid fibrils based on experimental constraints from solid state NMR. *Proc. Natl. Acad. Sci. USA*, **99**, 16742–16747.

20. Antzutkin, O. N., Balbach, J. J. & Tycko, R. (2003). Site-specific identification of non-beta-strand conformations in Alzheimer's beta-amyloid fibrils by solid-state NMR. *Biophys. J.* **84**, 3326–3335.

21. Kamihira, M., Oshiro, Y., Tuzi, S., Nosaka, A. Y., Saito, H. & Naito, A. (2003). Effect of electrostatic interaction on fibril formation of human calcitonin as studied by high resolution solid state C-13 NMR. *J. Biol. Chem.* **278**, 2859–2865.

22. Gordon, D. J., Balbach, J. J., Tycko, R. & Meredith, S. C. (2004). Increasing the amphiphilicity of an amyloidogenic peptide changes the beta-sheet structure in the fibrils from antiparallel to parallel. *Biophys. J.* **86**, 428–434.

23. Jaroniec, C. P., MacPhee, C. E., Bajaj, V. S., McMahon, M. T., Dobson, C. M. & Griffin, R. G. (2004). High-resolution molecular structure of a peptide in an amyloid fibril determined by magic angle spinning NMR spectroscopy. *Proc. Natl. Acad. Sci. USA*, **101**, 711–716.

24. Petkova, A. T., Buntkowsky, G., Dyda, F., Leapman, R. D., Yau, W. M. & Tycko, R. (2004). Solid state NMR reveals a pH-dependent antiparallel beta-sheet registry in fibrils formed by a beta-amyloid peptide. *J. Mol. Biol.* **335**, 247–260.

25. Chan, J. C. C., Oyler, N., Yau, W. M. & Tycko, R. (2005). Parallel beta-sheets and polar zippers in amyloid fibrils formed by residues 10–39 of the yeast prion protein Ure2p. *Biochemistry*, **44**, 10669–10680.

26. Chimon, S. & Ishii, Y. (2005). Capturing intermediate structures of Alzheimer's beta-amyloid, A beta(1–40), by solid-state NMR spectroscopy. *J. Am. Chem. Soc.* **127**, 13472–13473.

27. Heise, H., Hoyer, W., Becker, S., Andronesi, O. C., Riedel, D. & Baldus, M. (2005). Molecular-level secondary structure, polymorphism, and dynamics of full-length alpha-synuclein fibrils studied by solid-state NMR. *Proc. Natl. Acad. Sci. USA*, **102**, 15871–15876.

28. Masuda, Y., Irie, K., Murakami, K., Ohigashi, H., Ohashi, R., Takegoshi, K., Shimizu, T. & Shirasawa, T. (2005). Verification of the turn at positions 22 and 23 of the beta-amyloid fibrils with Italian mutation using solid-state NMR. *Bioorg. Med. Chem.* **13**, 6803–6809.

29. Petkova, A. T., Leapman, R. D., Guo, Z. H., Yau, W. M., Mattson, M. P. & Tycko, R. (2005). Self-propagating, molecular-level polymorphism in Alzheimer's beta-amyloid fibrils. *Science*, **307**, 262–265.

30. Ritter, C., Maddelein, M. L., Siemer, A. B., Luhrs, T., Ernst, M., Meier, B. H., Saupe, S. J. & Riek, R. (2005). Correlation of structural elements and infectivity of the HET-s prion. *Nature*, **435**, 844–848.

31. Siemer, A. B., Ritter, C., Ernst, M., Riek, R. & Meier, B. H. (2005). High-resolution solid-state NMR spectroscopy of the prion protein HET-s in its amyloid conformation. *Angew. Chem., Int. Ed. Engl.* **44**, 2441–2444.

32. Ferguson, N., Becker, J., Tidow, H., Tremmel, S., Sharpe, T. D., Krause, G. *et al.* (2006). General structural motifs of amyloid protofilaments. *Proc. Natl. Acad. Sci. USA*, **103**, 16248–16253.

33. Lim, K. H., Nguyen, T. N., Damo, S. M., Mazur, T., Ball, H. L., Prusiner, S. B. *et al.* (2006). Solid-state NMR structural studies of the fibril form of a mutant mouse prion peptide PrP89-143(P101L). *Solid State Nucl. Magn. Reson.* **29**, 183–190.

34. Paravastu, A. K., Petkova, A. T. & Tycko, R. (2006). Polymorphic fibril formation by residues 10–40 of the Alzheimer's beta-amyloid peptide. *Biophys. J.* **90**, 4618–4629.

35. Petkova, A. T., Yau, W. M. & Tycko, R. (2006). Experimental constraints on quaternary structure in Alzheimer's beta-amyloid fibrils. *Biochemistry*, **45**, 498–512.

36. Siemer, A. B., Arnold, A. A., Ritter, C., Westfeld, T., Ernst, M., Riek, R. & Meier, B. H. (2006). Observation of highly flexible residues in amyloid fibrils of the HET-s prion. *J. Am. Chem. Soc.* **128**, 13224–13228.

37. van der Wel, P. C. A., Lewandowski, J. R. & Griffin, R. G. (2007). Solid-state NMR study of amyloid

nanocrystals and fibrils formed by the peptide GNNQQNY from yeast prion protein Sup35p. *J. Am. Chem. Soc.* **129**, 5117–5130.

38. Kuwata, K., Matumoto, T., Cheng, H., Nagayama, K., James, T. L. & Roder, H. (2003). NMR-detected hydrogen exchange and molecular dynamics simulations provide structural insight into fibril formation of prion protein fragment 106–126. *Proc. Natl. Acad. Sci. USA*, **100**, 14790–14795.

39. Decatur, S. M. (2006). Elucidation of residue-level structure and dynamics of polypeptides via isotope-edited infrared spectroscopy. *Acc. Chem. Res.* **39**, 169–175.

40. Petty, S. A., Adalsteinsson, T. & Decatur, S. M. (2005). Correlations among morphology, ss-sheet stability, and molecular structure in prion peptide aggregates. *Biochemistry*, **44**, 4720–4726.

41. Petty, S. A. & Decatur, S. M. (2005). Intersheet rearrangement of polypeptides during nucleation of beta-sheet aggregates. *Proc. Natl. Acad. Sci. USA*, **102**, 14272–14277.

42. Silva, R. A. G. D., Barber-Armstrong, W. & Decatur, S. M. (2003). The organization and assembly of a beta-sheet formed by a prion peptide in solution: an isotope-edited FTIR study. *J. Am. Chem. Soc.* **125**, 13674–13675.

43. Sawaya, M. R., Sambashivan, S., Nelson, R., Ivanova, M. I., Sievers, S. A., Apostol, M. I. *et al.* (2007). Atomic structures of amyloid cross-beta spines reveal varied steric zippers. *Nature*, **447**, 453–457.

44. Yamada, N., Ariga, K., Naito, M., Matsubara, K. & Koyama, E. (1998). Regulation of beta-sheet structures within amyloid-like beta-sheet assemblage from tripeptide derivatives. *J. Am. Chem. Soc.* **120**, 12192–12199.

45. Fraser, P. E., Nguyen, J. T., Inouye, H., Surewicz, W. K., Selkoe, D. J., Podlisny, M. B. & Kirschner, D. A. (1992). Fibril formation by primate, rodent, and Dutch-hemorrhagic analogs of Alzheimer amyloid beta-protein. *Biochemistry*, **31**, 10716–10723.

46. Wishart, D. S., Bigam, C. G., Holm, A., Hodges, R. S. & Sykes, B. D. (1995). 1H, 13C and 15N random coil NMR chemical shifts of the common amino acids. I. Investigation of nearest-neighbor effects. *J. Biomol. NMR*, **5**, 67–81.

47. Mou, Y., Tsai, T. W. T. & Chan, J. C. C. (2007). Determination of the backbone torsion psi angle by tensor correlation of chemical shift anisotropy and heteronuclear dipole–dipole interaction. *Solid State Nucl. Magn. Reson.* **31**, 72–81.

48. Lehmann, M. S., Koetzle, T. F. & Hamilton, W. C. (1972). Precision neutron diffraction structure determination of protein and nucleic acid components. I. The crystal and molecular structure of the amino acid L-alanine. *J. Am. Chem. Soc.* **94**, 2657–2660.

49. Carroll, P. J., Stewart, P. L. & Opella, S. J. (1990). Structures of two model peptides—*N*-acetyl-D,L-valine and *N*-acetyl-L-valyl-L-leucine. *Acta Crystallogr., Sect. C: Cryst. Struct. Commun.* **46**, 243–246.

50. Mou, Y., Chen, P. H., Lee, S. W. & Chan, J. C. C. (2007). Determination of chemical shift anisotropies of unresolved carbonyl sites by C-alpha detection under magic angle spinning. *J. Magn. Reson.* **187**, 352–356.

51. Ishii, Y., Terao, T. & Kainosho, M. (1996). Relayed anisotropy correlation NMR: determination of dihedral angles in solids. *Chem. Phys. Lett.* **256**, 133–140.

52. Feng, X., Verdegem, P. J. E., Eden, M., Sandstrom, D., Lee, Y. K., Bovee-Geurts, P. H. M., de Grip, W. J.,
Lugtenburg, J., de Groot, H. J. M. & Levitt, M. H. (2000). Determination of a molecular torsional angle in the metarhodopsin-I photointermediate of rhodopsin by double-quantum solid-state NMR. *J. Biomol. NMR*, **16**, 1–8.

53. Gullion, T. & Schaefer, J. (1989). Rotational-echo double-resonance NMR. *J. Magn. Reson.* **81**, 196–200.

54. Antzutkin, O. N., Leapman, R. D., Balbach, J. J. & Tycko, R. (2002). Supramolecular structural constraints on Alzheimer's beta-amyloid fibrils from electron microscopy and solid-state nuclear magnetic resonance. *Biochemistry*, **41**, 15436–15450.

55. Ishii, Y., Balbach, J. J. & Tycko, R. (2001). Measurement of dipole-coupled lineshapes in a many-spin system by constant-time two-dimensional solid state NMR with high-speed magic-angle spinning. *Chem. Phys.* **266**, 231–236.

56. Nelson, R., Sawaya, M. R., Balbirnie, M., Madsen, A. O., Riekel, C., Grothe, R. & Eisenberg, D. (2005). Structure of the cross-beta spine of amyloid-like fibrils. *Nature*, **435**, 773–778.

57. Cornilescu, G., Delaglio, F. & Bax, A. (1999). Protein backbone angle restraints from searching a database for chemical shift and sequence homology. *J. Biomol. NMR*, **13**, 289–302.

58. Feng, X., Lee, Y. K., Sandstrom, D., Eden, M., Maisel, H., Sebald, A. & Levitt, M. H. (1996). Direct determination of a molecular torsional angle by solid-state NMR. *Chem. Phys. Lett.* **257**, 314–320.

59. Henrichs, P. M. & Linder, M. (1985). Use of carbon–carbon nuclear-spin diffusion for the study of the miscibility of polymer blends. *J. Magn. Reson.* **58**, 458.

60. Robyr, P., Meier, B. H., Fischer, P. & Ernst, R. R. (1994). A combined structural study using NMR chemical-shielding-tensor correlation and neutron-diffraction in polycrystalline methanol. *J. Am. Chem. Soc.* **116**, 5315.

61. Schmidt-Rohr, K. (1996). Torsion angle determination in solid $^{13}$C-labeled amino acids and peptides by separated-local-field double-quantum NMR. *J. Am. Chem. Soc.* **118**, 7601–7603.

62. Tycko, R. & Dabbagh, G. (1991). Nuclear-magnetic-resonance crystallography—molecular orientational ordering in 3 forms of solid methanol. *J. Am. Chem. Soc.* **113**, 3592–3593.

63. Blanco, F. J. & Tycko, R. (2001). Determination of polypeptide backbone dihedral angles in solid state NMR by double quantum C-13 chemical shift anisotropy measurements. *J. Magn. Reson.* **149**, 131–138.

64. Bower, P. V., Oyler, N., Mehta, M. A., Long, J. R., Stayton, P. S. & Drobny, G. P. (1999). Determination of torsion angles in proteins and peptides using solid state NMR. *J. Am. Chem. Soc.* **121**, 8373–8375.

65. Costa, P. R., Gross, J. D., Hong, M. & Griffin, R. G. (1997). Solid-state NMR measurement of psi in peptides: a NCCN 2Q-heteronuclear local field experiment. *Chem. Phys. Lett.* **280**, 95–103.

66. Eden, M., Brinkmann, A., Luthman, H., Eriksson, L. & Levitt, M. H. (2000). Determination of molecular geometry by high-order multiple-quantum evolution in solid-state NMR. *J. Magn. Reson.* **144**, 266–279.

67. Feng, X., Eden, M., Brinkmann, A., Luthman, H., Eriksson, L., Graslund, A. *et al.* (1997). Direct determination of a peptide torsional angle psi by double-quantum solid-state NMR. *J. Am. Chem. Soc.* **119**, 12006–12007.

68. Ladizhansky, V., Veshtort, M. & Griffin, R. G. (2002). NMR determination of the torsion angle psi in alpha-helical peptides and proteins: the HCCN dipolar correlation experiment. *J. Magn. Reson.* **154**, 317–324.

69. Reif, B., Hohwy, M., Jaroniec, C. P., Rienstra, C. M. & Griffin, R. G. (2000). NH–NH vector correlation in peptides by solid-state NMR. *J. Magn. Reson.* **145**, 132–141.

70. Rienstra, C. M., Hohwy, M., Mueller, L. J., Jaroniec, C. P., Reif, B. & Griffin, R. G. (2002). Determination of multiple torsion-angle constraints in U-C-13,N-15-labeled peptides: 3D H-1-N-15-C-13-H-1 dipolar chemical shift NMR spectroscopy in rotating solids. *J. Am. Chem. Soc.* **124**, 11908–11922.

71. Chan, J. C. C. & Tycko, R. (2003). Solid-state NMR spectroscopy method for determination of the backbone torsion angle psi in peptides with isolated uniformly labeled residues. *J. Am. Chem. Soc.* **125**, 11828–11829.

72. Ma, B. & Nussinov, R. (2002). Molecular dynamics simulations of alanine rich beta-sheet oligomers: insight into amyloid formation. *Protein Sci.* **11**, 2335–2350.

73. Hediger, S., Meier, B. H., Kurur, N. D., Bodenhausen, G. & Ernst, R. R. (1994). NMR cross-polarization by adiabatic passage through the Hartmann–Hahn condition (Aphh). *Chem. Phys. Lett.* **223**, 283–288.

74. Hediger, S., Meier, B. H. & Ernst, R. R. (1995). Adiabatic passage Hartmann–Hahn cross-polarization in NMR under magic-angle sample-spinning. *Chem. Phys. Lett.* **240**, 449–456.

75. Detken, A., Hardy, E. H., Ernst, M. & Meier, B. H. (2002). Simple and efficient decoupling in magic-angle spinning solid-state NMR: the XiX scheme. *Chem. Phys. Lett.* **356**, 298–304.

76. Ishii, Y. (2001). C-13–C-13 dipolar recoupling under very fast magic angle spinning in solid-state nuclear magnetic resonance: applications to distance measurements, spectral assignments, and high-throughput secondary-structure determination. *J. Chem. Phys.* **114**, 8473–8483.

77. Delaglio, F., Grzesiek, S., Vuister, G. W., Zhu, G., Pfeifer, J. & Bax, A. (1995). NMRPipe—a multidimensional spectral processing system based on UNIX pipes. *J. Biomol. NMR*, **6**, 277–293.

78. Levitt, M. H. (2002). Symmetry-based pulse sequence in magic-angle spinning solid-state NMR. In (Grant, D. M. & Harris, R. K., eds), *Encyclopedia in Nuclear Magnetic Resonance*, vol. 9, pp. 165–196. Wiley, Chichester.

79. Chan, J. C. C. & Brunklaus, G. (2001). R sequences for the scalar-coupling mediated homonuclear correlation spectroscopy under fast magic-angle spinning. *Chem. Phys. Lett.* **349**, 104–112.

80. Mou, Y., Chao, J. C. H. & Chan, J. C. C. (2006). Efficient spin–spin scalar coupling mediated C-13 homonuclear polarization transfer in biological solids without proton decoupling. *Solid State Nucl. Magn. Reson.* **29**, 278–282.

81. Lee, M. & Goldburg, W. I. (1965). Nuclear-magnetic-resonance line narrowing by a rotating rf field. *Phys. Rev. A*, **140**, 1261.

82. Anderson, R. C., Gullion, T., Joers, J. M., Shapiro, M., Villhauer, E. B. & Weber, H. P. (1995). Conformation of [1-C-13,N-15]acetyl-L-carnitine-rotational-echo, double-resonance nuclear-magnetic-resonance spectroscopy. *J. Am. Chem. Soc.* **117**, 10546–10550.

83. Bennett, A. E., Rienstra, C. M., Auger, M., Lakshmi, K. V. & Griffin, R. G. (1995). Heteronuclear decoupling in rotating solids. *J. Chem. Phys.* **103**, 6951–6958.

84. Bak, M., Rasmussen, J. T. & Nielsen, N. C. (2000). SIMPSON: a general simulation program for solid-state NMR spectroscopy. *J. Magn. Reson.* **147**, 296–330.

85. Veshtort, M. & Griffin, R. G. (2006). SPINEVOLUTION: a powerful tool for the simulation of solid and liquid state NMR experiments. *J. Magn. Reson.* **178**, 248–282.

86. Bak, M. & Nielsen, N. C. (1997). REPULSION, a novel approach to efficient powder averaging in solid-state NMR. *J. Magn. Reson.* **125**, 132–139.

87. Ponder, J. W. (2004). TINKER Version 4.2, Tinker Software Tools for Molecular Design.

88. Cornell, W. D., Cieplak, P., Bayly, C. I., Gould, I. R., Merz, K. M., Ferguson, D. M. *et al.* (1995). A 2nd generation force-field for the simulation of proteins, nucleic-acids, and organic-molecules. *J. Am. Chem. Soc.* **117**, 5179–5197.

89. Ooi, T., Oobatake, M., Nemethy, G. & Scheraga, H. A. (1987). Accessible surface-areas as a measure of the thermodynamic parameters of hydration of peptides. *Proc. Natl. Acad. Sci. USA*, **84**, 3086–3090.

90. Essmann, U., Perera, L., Berkowitz, M. L., Darden, T., Lee, H. & Pedersen, L. G. (1995). A smooth particle mesh Ewald method. *J. Chem. Phys.* **103**, 8577–8593.

91. Andersen, H. C. (1983). Rattle—a velocity version of the shake algorithm for molecular-dynamics calculations. *J. Comput. Phys.* **52**, 24–34.